*Desalination and Water Treatment*
www.deswater.com

doi: 10.5004/dwt.2020.26445

208 (2020) 32–42
December

# Improvement of poly(piperazine-amide) composite nanofiltration membranes by incorporating of hollow polypyrrole nanospheres with mesoporous shells

Xiaoli Ding[a,b,c], Xiaofeng Li[a,b,c], Hongyong Zhao[a,b,d,*], Jingwen Yao[a,b,c], Yuzhong Zhang[a,b,c,*]

[a]*State Key Laboratory of Separation Membranes and Membrane Processes/National Center for International Joint Research on Separation Membranes, Tiangong University, Tianjin 300387, China, emails: zhaohongyong@tiangong.edu.cn (H. Zhao), zhangyz2004cn@vip.163.com (Y. Zhang), dingxiaoli@tiangong.edu.cn (X. Ding), 1223946396@qq.com (X. Li), 2207518497@qq.com (J. Yao)*
[b]*Tianjin Key Laboratory of Hollow Fiber Membrane Materials and Processes (Tiangong University), Tianjin 300387, China*
[c]*School of Material Science and Engineering, Tiangong University, Tianjin 300387, China*
[d]*School of Chemistry and Chemical Engineering, Tiangong University, Tianjin 300387, China*

Received 23 February 2020; Accepted 8 August 2020

**ABSTRACT**

Incorporation of nanospheres into membranes is a potential strategy to improve the performance of the nanofiltration membranes, including permeation/separation performance and antifouling performance. In this study, we used the hollow polypyrrole nanospheres with mesoporous shells as fillers in a selective layer to prepare poly(piperazine amide) composite nanofiltration membranes by interfacial polymerization. The effects of the hollow nanospheres with mesoporous shells on the physical properties of the membrane surfaces (water contact angle, zeta potential, and roughness), permeability, rejection of inorganic salts, and antifouling performance against humic acid were investigated. The incorporation of the hollow polypyrrole nanospheres increased permeability with a pure water flux increasing from 43.9 to 90.1 L $m^{-2}$ $h^{-1}$ at 0.5 MPa without a significant decrease in rejection. The rejection of modified membranes was up to 99.7% for $Na_2SO_4$, 99.4% for $MgSO_4$, 68.7% for $MgCl_2$, and 49.3% for NaCl. The antifouling property against humic acid was also improved owing to the increased hydrophilicity.

*Keywords:* Nanofiltration; Composite membrane; Mixed matrix membrane; Hollow nanosphere

## 1. Introduction

Nanofiltration (NF) has been widely used in water treatment due to its advantages in simplicity and less energy consumption, etc. However, NF membranes, which are mainly manufactured by polymers are also troubled by the "trade-off" effect between flux and rejection [1], the same as the gas separation membrane material. Besides using mixed monomers [2], the incorporation of nanomaterials into polymer matrice to form mixed matrix membranes (MMMs) is another crucial strategy to the current bottlenecks from the balance between flux and rejection, which improves the permeation and separation performance generally by disturbing the package of the polymer chain [3]. Additionally, incorporating nanomaterials also improves some other physical properties such as hydrophilicity, roughness, and the antifouling property of membranes.

Recently, a considerable variety of nanomaterials have been incorporated into selective layers to prepare composite nanofiltration membranes. The nanomaterials are generally divided into three types: (1) nonporous nanomaterials, including three-dimensional nanoparticles (e.g., metal and metal oxide nanoparticles [4], polymer nanoparticles [5,6]), two-dimensional nanoplates (e.g., graphene oxide (GO) and

* Corresponding authors.

1944-3994/1944-3986 © 2020 Desalination Publications. All rights reserved.

the derivers [7,8], boron nitride nanosheet [9]), and zero-dimensional quantum dots [10]; (2) porous nanomaterials, including clay [11], zeolite [12], metal-organic frameworks [13,14], and porous organic framework [15,16]; (3) hollow nanomaterials, such as carbon nanotube (CNT) [17–19], halloysite nanotube [20–22], and trititanate nanotube [23]. The incorporation of non-porous nanomaterials improves the permeation mainly by disturbing the package of polymer chain or increasing the hydrophilic property [3,4,7]. Additionally, the two-dimension nanoplates can form adjustable laminar nanochannels for potential fast water transport. Typically, the pore of porous nanomaterials and the inner pores of hollow nanomaterials tend to act as selective nanopores and preferential flow paths for water and solvent, thereby, the hollow and porous nanomaterials-filled membranes show the enhanced flux without sacrifice of rejection [24,25]. For example, the flux through CNTs has been estimated to be 3–4 orders of magnitude faster than though compact polyamide predicted by the Hagen–Poiseuille equation [17]. However, the agglomeration of nanotubes due to the weak polymer-tube adhesion leads to defects and then a poor separation performance [26]. Compared to the polymeric matrix/inorganic filler combination, the polymeric matrix/organic filler combination has greater flexibility for membrane formation, and the better compatibility between matrice and fillers makes it particularly suitable for preparing MMMs [5]. While the nanofiltration membranes doped with hollow polymer nanoparticles have received little coverage. As such, in this study, we synthesized hollow polypyrrole nanospheres (HPNs) with mesoporous shells as the filler to prepare composite membranes with a mixed matrix selective layer based on poly(piperazine amide). Besides the compatibility of fillers with the polymeric matrix, the hollow nanospheres with mesopores in shells evade the other drawback induced by inorganic nanotubes, that is the impermeability of the tube wall in the current research, requires the vertical arrangement of the tube on the membrane surface to obtain the optimal performance [27].

## 2. Experimental

### 2.1. Materials

The HPNs were synthesized in our laboratory with an average diameter of 33 nm. The hollow nanospheres have mesopores in the polypyrrole shell with the most probable diameter of 2.17 nm. The details of the synthesis process and the structure were described elsewhere [28]. The polysulfone (PSf) substrate membrane coated on the nonwoven fabric was also fabricated in our laboratory by non-solvent induced phase separation, displaying a pure water flux of 400.0 L $m^{-2}$ $h^{-1}$ at 0.1 MPa with a molecular weight cutoff of 43 kDa. Trimesoyl chloride (TMC, 98%, Heowns, China), piperazine (PIP, AR, Kermel, China), *n*-hexane (AR, Kermel, China), magnesium sulfate ($MgSO_4$, AR, Tianjin Fengchuang Chemical Reagent Technologies Co., Ltd., China), sodium chloride (NaCl, AR, Tianjin Damao Chemical Reagent Factory, China), magnesium chloride ($MgCl_2$, AR, Tianjin Guangfu Fine Chemical Research Institute, China), sodium sulfate ($Na_2SO_4$, AR, Tianjin Damao Chemical Reagent Factory, China), humid acid (HA, 95%, Tianjin Guangfu Fine Chemical Research Institute, China), citric acid (97%, Tianjin Guangfu Fine Chemical Research Institute, China), sodium hydroxide (96%, Tianjin Guangfu Fine Chemical Research Institute, China), and polyethylene glycol (AR, Kermel, China) were used as received.

### 2.2. Membrane fabrication

The selective layer of the composite membrane was synthesized on the PSf substrate membrane by interface polymerization. The HPNs were dispersed into 0.8 w/v% PIP/water solution by sonication for 30 min (KQ100DB, Kunshan Ultrasonic Instruments, China). The PIP/water/HPNs mixture with various concentration of HPNs (w/v%) was poured onto the top surface of substrate membranes for 4 min, and then the excess solution on the surface was carefully removed by a rubber roller. Subsequently, TMC/*n*-hexane solution (0.1 w/v%) was poured onto the substrate membrane soaked by PIP solution for 1 min to form the selective layer. After being washed in *n*-hexane to remove the unreacted TMC, the nascent composite membrane was heated in oven at 70°C for 10 min to obtain the composite membrane. The whole process is presented in Fig. 1.

### 2.3. Membranes characterization

The reaction between TMC and PIP was confirmed by attenuated total reflection Fourier transform infrared spectroscopy (FTIR-ATR, Bruker Vector-22, Germany), with the sample scanned at 4 $cm^{-1}$ resolution from 400 to 4,000 $cm^{-1}$ range. The surface elemental content of membranes was characterized by X-ray photoelectron spectroscopy (XPS, Thermofisher, America), which can be also used to confirm the reaction between PIP and TMC. The surface and cross-section morphologies of the membranes were studied by Field emission scanning electron microscope (FESEM, Hitachi S-4800, Japan). The surface roughness of the membranes was determined by atomic force microscopy (AFM, Nanoscope 3, Agilent, America). The surface charge property of composite membranes quantified as zeta potential (mV) was determined by zeta potential analysis meter (Anton Paar, SurPASS, Austria) at 25°C. The contact angle (°) of the pure water on the membrane surface, characterizing the hydrophilicity of the membrane surface, was determined by contact angle meter (JC-2000C1, powereach[å], China). The wide angle X-ray diffraction (WAXD) patterns obtained by using a Scintag theta–theta diffractometer (Bruker AXS, D8 Advanced, Germany) were used to characterize the average inter-segmental distance of polymer chains (*d*-spacing, nm), calculated by Bragg's Law as the following equation:

$$d=\frac{\lambda}{2\sin\theta} \tag{1}$$

where $\lambda$ is the wavelength of Cu K$\alpha$ radiation (1.54 Å), $\theta$ (°) is the broad peak center in the WAXD pattern.

The permeation and separation performances of the composite membranes were characterized by measuring the pure water flux (PWF, L $m^{-2}$ $h^{-1}$) and inorganic salt rejections ($R$). Salt solutions containing NaCl, $MgSO_4$, $Na_2SO_4$, and $MgCl_2$ (1 g $L^{-1}$), respectively, were used as the feed solution.

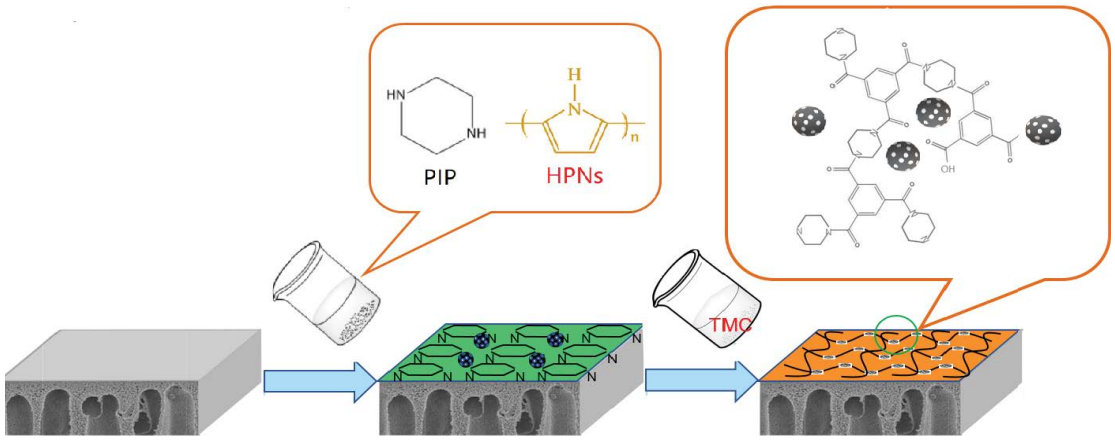


Fig. 1. Process of MMMs preparation.

The nanofiltration experiment was conducted by using a laboratory-scale cross-flow filtration system with an effective area of 19.6 cm$^2$. The membranes were pre-compressed with pure water at 0.8 MPa for 20 min. Then, the flux and rejections were evaluated at trans-membrane pressures up to 0.5 MPa at room temperature. Flux was calculated using the following equation:

$$\text{Flux} = \frac{V}{At} \tag{2}$$

where $V$ (L) is the water volume collected in the permeate side, fixed at 10 × 10$^{-3}$ L in this study, $A$ (m$^2$) is the effective membrane area, and $t$ (h) is the collection time.

The rejection was calculated using the following equation:

$$R = \left(1 - \frac{C_p}{C_f}\right) \times 100\% \tag{3}$$

where $C_p$ (mol L$^{-1}$) and $C_f$ (mol L$^{-1}$) are the salt concentrations in the permeate and feed solution respectively, determined from the conductivity measured by an electrical conductivity (DDS-11A, Shanghai INESA Scientific Instrument Co., Ltd., China). PWF, rejection, and the contact angle were measured for three times, then averaged the results. The molecular weight cutoff was determined by polyethylene glycol rejection and the concentration of polyethylene glycol was measured by a TOC analyzer (Phoenix 8000, Tekamr-Dohrmann, America). The pore size of the composite membrane was characterized by Stokes radius, which was calculated as the flowing equation:

$$\log r_s = -1.4854 + 0.461 \log M \tag{4}$$

where $r_s$ (nm) is the Stokes radius of the solute and $M$ (g mol$^{-1}$) is molecular weight cutoff [29]. Polyethylene glycol solutions with a concentration of 1,000 ppm were used to test under 0.6 MPa.

The physical stability of the composite membranes was assessed by conducting the filtration experiment in pure water at 0.5 MPa for 840 min. The antifouling performance was evaluated by conducting the filtration experiment in HA solution (40 mg L$^{-1}$) for 840 min and comparing the normalized flux (the real-time flux/the initial flux) of HA solution with that of pure water. Following fouling experiments, the cleaning process was carried out by using pure water, 2 wt.% citric acid solution, and 0.1 wt.% NaOH solution as the cleaning agent respectively, each for 90 min. The flux recovery ratio was defined and calculated using the following equation to evaluate the cleaning effect:

$$\text{FRR} = \frac{J_{w2}}{J_{w1}} \times 100\% \tag{5}$$

where $J_{w2}$ (L m$^{-2}$ h$^{-1}$) is the water flux tested after backwashing, $J_{w1}$ (L m$^{-2}$ h$^{-1}$) is the initial flux.

## 3. Result and discussion

### 3.1. Characterization of membranes

#### 3.1.1. Surface chemistry of membranes

The reaction between PIP and TMC was confirmed by FTIR as shown in Fig. 2. The characteristic bands at ~1,320 and 1,296 cm$^{-1}$ were assigned to the O=S=O asymmetric stretching vibration in PSf, bands at ~1,151 and 1,167 cm$^{-1}$ were assigned to the O=S=O symmetric stretching vibration. The characteristic bands of PSf were also founded in the spectra of composite membranes, indicating the thin polyamide layer. The amide-I bands at ~1,660 cm$^{-1}$ and amide-III bands at ~1,240 cm$^{-1}$ appeared in the spectra of composite membranes, while the amide-II bands at ~1,540 cm$^{-1}$ absented, indicating the formation of the poly(piperazine amide) [30]. The bands at 1,460 and 1,553 cm$^{-1}$ corresponded to the C–N stretching vibration in the ring of polypyrrole. The band at 1,033 cm$^{-1}$ was due to in-plane deformation of N–H bond of pyrrole ring, the band at 948 cm$^{-1}$ was assigned to the C–H deformation vibration in the CH=CH group [31]. There was no significant difference between the spectrum of unmodified composite membranes and that of modified composite membranes, which might because the HPNs were embedded in the polymer chain.

XPS analysis was conducted to further determine the surface elemental compositions of membrane surfaces as

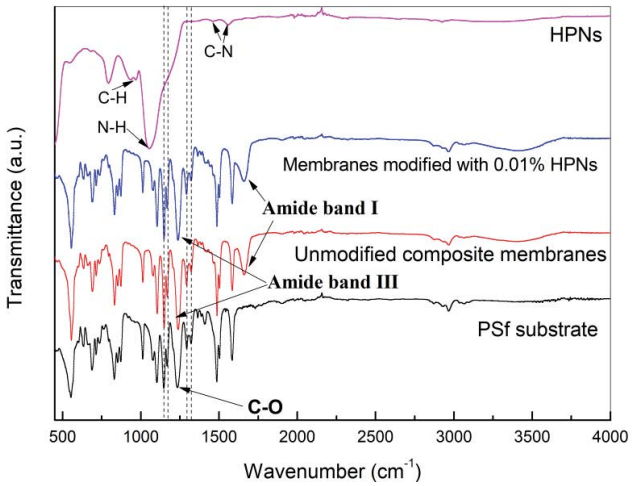


Fig. 2. FTIR spectra of the membranes and the HPNs.

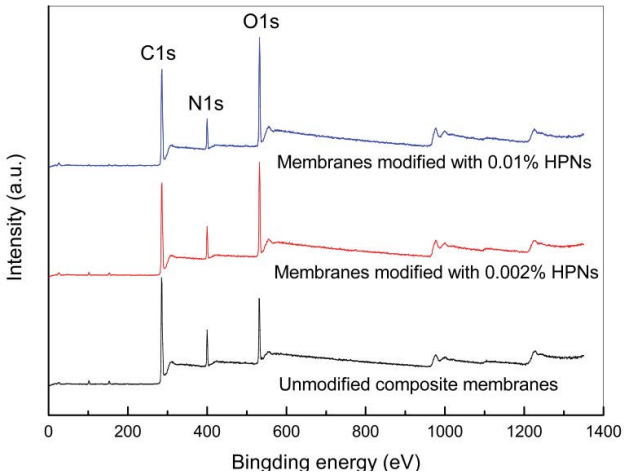


Fig. 3. XPS spectra of composite membranes.

shown in Fig. 3 and Table 1. The modification with HPNs decreased the atomic percentage of N, because of the lower percentage of N in polypyrrole. The modification with HPNs increased the atomic percentages of O and C, then obviously increased the ratio of the atomic percentage of O to N, indicating that the introducing of the HPNs decreased the cross-linking degree of poly(piperazine amide), because the increased O mainly came from the carboxyl groups hydrolyzed from unreacted acyl chloride groups.

### 3.1.2. Morphology of membranes

The FESEM images of the membranes are presented in Fig. 4. All the membranes including PSf substrate, the poly(piperazine-amide) composite membrane without modification, and composite membranes modified with HPNs, were asymmetric structures. The PSf substrate was consisted by finger-like voids and sponge-like layer. The selective layers of composite membranes were attached to the sponge-like layer with the similar thickness of about 90 nm. The surface of the PSf substrate was porous structure with a pore diameter of 50–100 nm. The morphology of the surface of the pure polyamide skin was the typical morphology of the PIP/TMC membrane, with the intense grainy and convex structures in the rough surface [32]. Compared with the unmodified membrane, the grain of MMMs increased in size because the HNPs in the PIP solution blocked the diffusion of the PIP and TMC and then decreased the concentration gradient [33]. In MMMs, the HPNs could be observed as white spots in the FESEM images. At lower loading (0.002%), the HPNs were well dispersed on the surface with a diameter of ~25 nm, indicating no aggregation. And most of them were scattered in the valley and some were scattered at the peak. From the FESEM images, we could found that the grain formed by PIP/TMC measured 100–200 nm across, and the HPNs measured ~25 nm across, indicating the formation of the submicro/nano structure, which might affect the surface roughness, the wetting property and then the antifouling performance, etc. At higher loading (0.01%), we found some HPNs aggregated together to form large clusters. Fig. 4d shows the wrinkled surface around the clusters of the HPNs. The stress due to the polymerization concentrated on HPNs, and resulting in the wrinkled surface. The topography of membrane surfaces was determined by AFM as displayed in Fig. 5. The average roughness ($R_a$) as presented in Fig. 5, increased as the HPNs loading increased, which was consistent with the other results obtained from other reports [8,21]. The bumps in AFM images of membranes modified with HPNs further confirmed the wrinkled surface.

### 3.1.3. Physical properties of membrane surfaces

The surface hydrophilicity of the prepared composite membranes was studied in terms of the water contact angle as presented in Fig. 6. The addition of the HPNs decreased the water static contact angle, indicating the increase in hydrophilicity of composite membranes. Generally, the contract angle is mainly governed by the surface chemical composition and the surface microstructure [34,35]. In this study, the flat polypyrrole surface had a higher contact

Table 1
XPS results of composite membranes

| Membranes | Atomic percentage (%) | | | Atomic ratio | |
|---|---|---|---|---|---|
| | O | N | C | O/N | C/N |
| Unmodified | 15.42 | 10.51 | 71.18 | 1.47 | 6.77 |
| Modified with 0.002% HPNs | 22.29 | 9.36 | 66.51 | 2.37 | 7.08 |
| Modified with 0.01% HPNs | 24.05 | 8.79 | 66.37 | 2.74 | 7.55 |

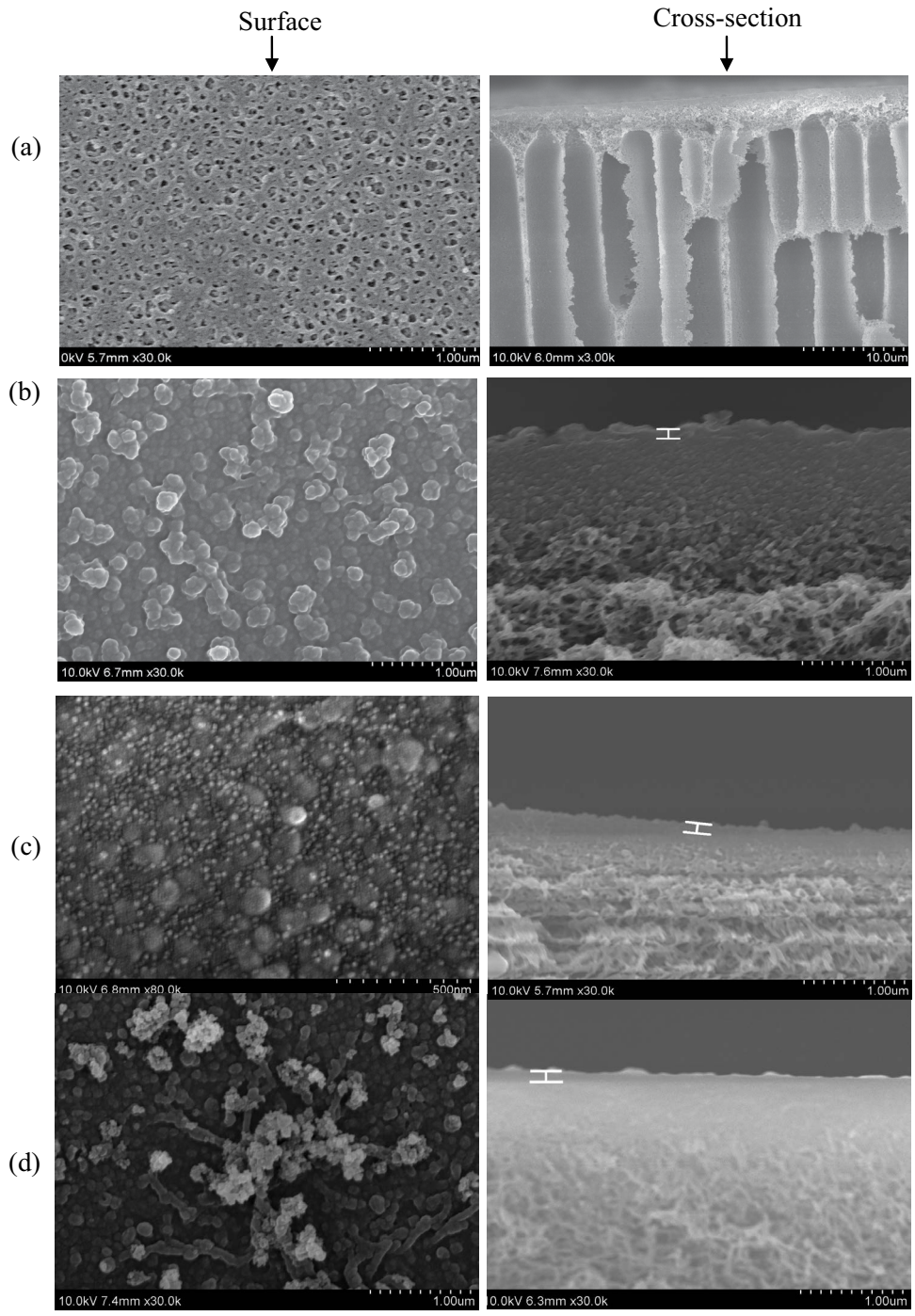


Fig. 4. FESEM images of the membranes. (a) PSf substrate, (b) unmodified composite membrane, (c) composite membrane modified with 0.002% HPNs and (d) composite membrane modified with 0.01% HPNs.

angle (73°) than the surface of the unmodified PIP based composite membranes [36]. That was to say the changes of the chemical composition induced by incorporation of HNPs had the negative effect on the hydrophilicity. As presented in Fig. 5, the topographic roughness of membrane increased as the HPNs loading increased, and the membrane surface formed the submicro/nano structure as shown in Fig. 4, which had the positive effect on hydrophilicity. Obviously, in this study, the positive effect of the surface microstructure overcame the negative effect of the surface composition, resulting in the decreased contact angle and then the improved hydrophilicity. The surface charge of the prepared composite membranes was studied in terms of the surface zeta potential at different pH values as presented in Fig. 7. Due to the positive change from the HPNs, the incorporation of HPNs decreased the zeta potential, which might

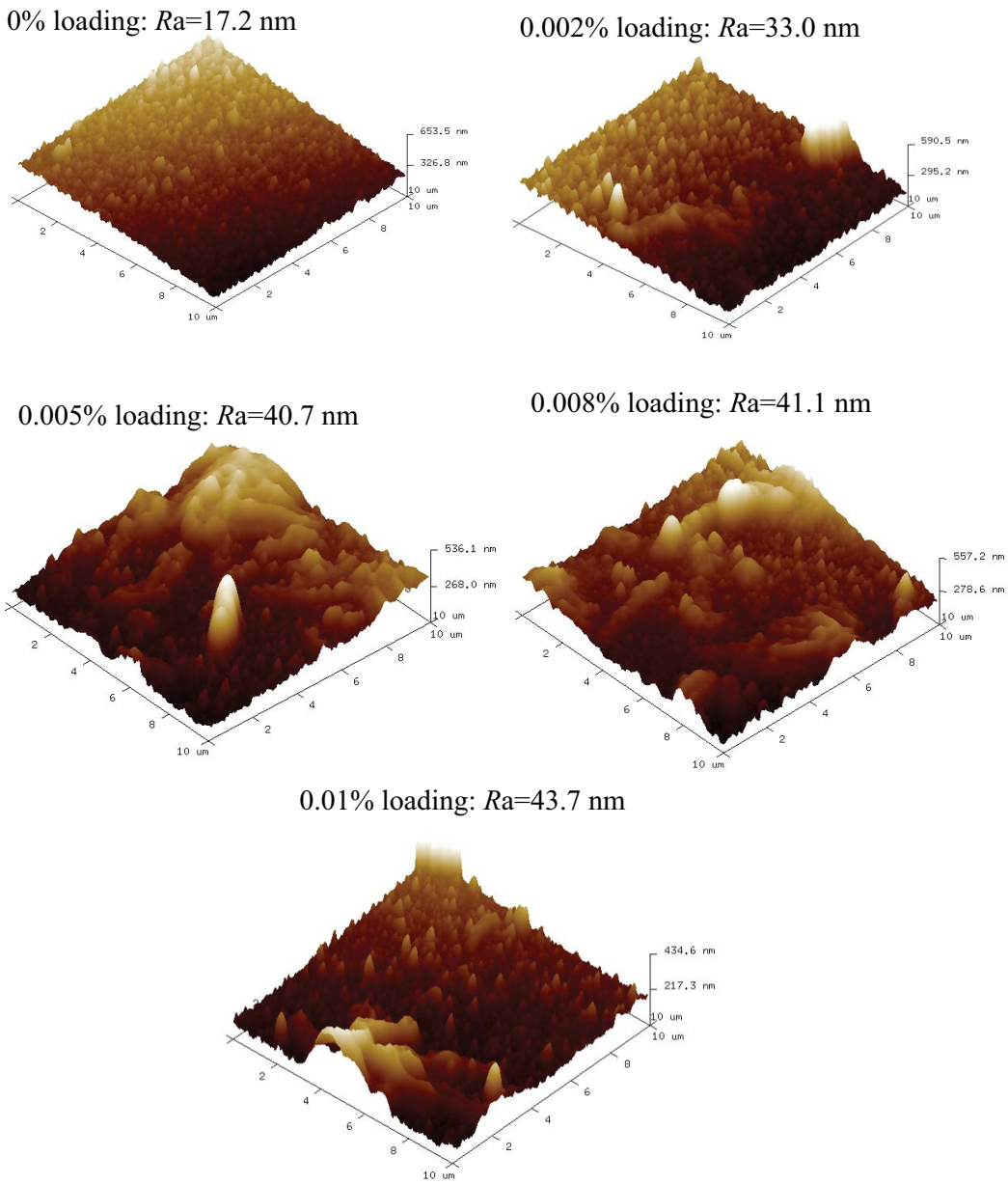


Fig. 5. AFM images of the composite membranes.

adversely affect the separation performance of inorganic salt or other charged solute and the antifouling performance. The WAXD spectra of unmodified composite membranes and MMMs modified with 0.01% HPNs are presented in Fig. 8. The incorporation of HPNs induced a slight shift of the peak from 17.6° to 17.5°, that was to say the *d*-spacing increased slightly, indicating a slightly lower degree of cross-linking, which was consistent with the XPS results.

### *3.2. Permeation and separation performances of membranes*

The pure water fluxes of the composite membranes are presented in Fig. 9. The incorporation of HPNs increased the pure water flux. The pure water flux significantly increased at low HPNs loading. When the composite membrane was modified with 0.002% HPNs, the flux increased by 50% from 43.9 to 65.7 L $m^{-2}$ $h^{-1}$, while the growth slowed down as the HPNs loading continued to increase, because of the aggregation of HPNs as shown in Fig. 4. Compared with that of composite membranes modified with 0.008% HPNs, the pure water flux of composite membranes modified with 0.01% HPNs only increased by 1.3%. Generally, the improvement of the flux for MMMs was mainly due to the disruption of the package of the polymer chain and the improved hydrophilicity. In addition, the hollow structure of the fillers provided the feasible channel for transport and then increased the flux. In this study, we did not observe the significant change in the package of the polymer chain as shown in Fig. 8. Therefore, the improved hydrophilicity and the extra channels might play the leading roles.

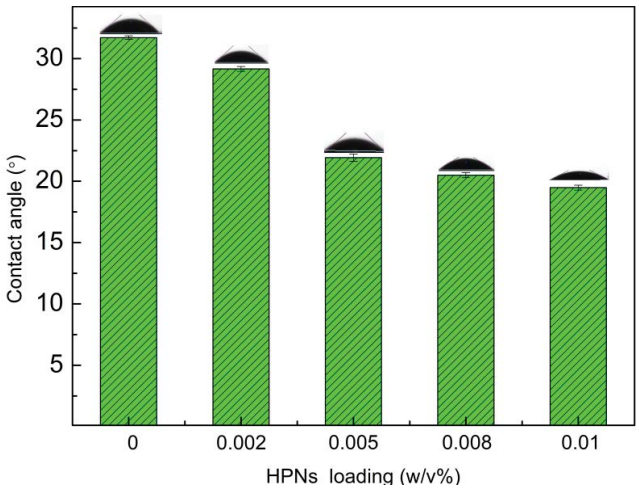


Fig. 6. Water contact angle of the membrane surface.

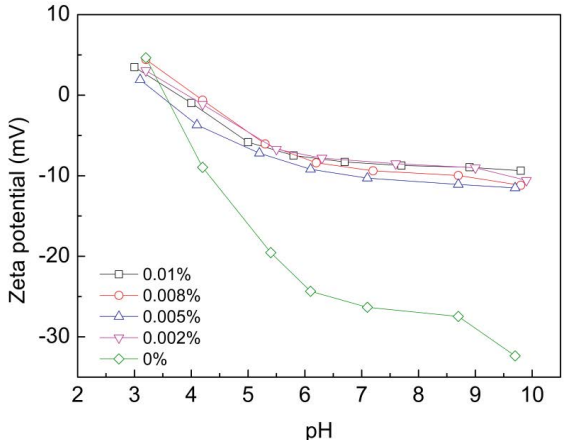


Fig. 7. Surface zeta potentials of the prepared composite membranes modified with different HPNs at different pH values.

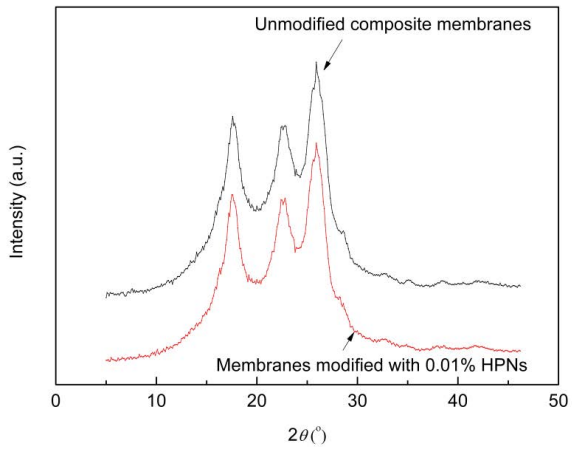


Fig. 8. WAXD patterns of the unmodified composite membranes and composite membranes modified with 0.01% HPNs.

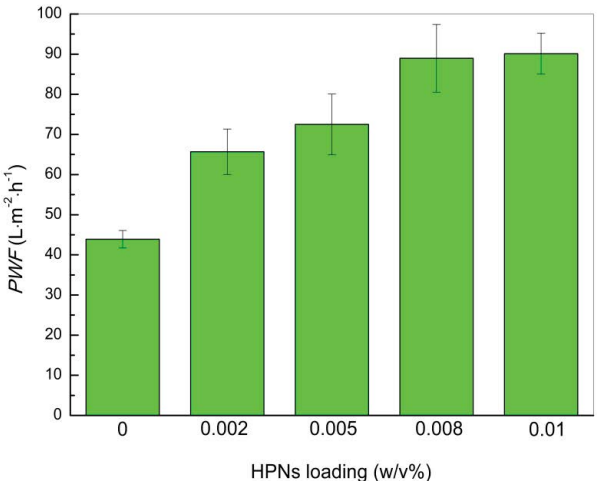


Fig. 9. Effect of the HPNs on the pure water flux of the composite membranes.

The rejections of inorganic salts for the composite membranes are presented in Fig. 10. The membranes showed excellent rejection properties of all the salts with the $Na_2SO_4$ rejection of 98.9%–99.6%, the $MgSO_4$ rejection of 97.8%–99.5%, the $MgCl_2$ rejection of 64.9%–68.7%, and the NaCl rejection of 42.4%–49.2%. The rejection performance of all the composite membranes to the different inorganic salts followed the order of $Na_2SO_4$ > $MgSO_4$ > $MgCl_2$ > NaCl, which was typical for negatively charged nanofiltration membranes [37]. The rejections changed insignificantly by the addition of the HPNs, except the NaCl rejection with an increase of about 12%, which was the result of many factors. On one hand, the increase of the water flux would increase the rejections. On the other hand, in this study, the Donnan exclusion and steric hindrance which are well known as the separation mechanisms for inorganic salts in nanofiltration membranes, would cause the decrease in rejections. HPNs in the membranes neutralized the surface electricity and then decreased the surface electronegativity as shown in Fig. 7, which made the modified membranes less resistance toward permeating the anions, especially the divalent anions. Therefore, the rejections would decrease. Additionally, the decrease of the degree of cross-linking due to the addition of HPNs, which was confirmed by XPS result in Fig. 3 and Table 1, would decrease the rejections. Compared with the divalent ions, the Donnan exclusion and steric hindrance had less influence on monovalent ions, thus, the rejection of NaCl for modified membranes increased, others fluctuated in a narrow range. All the composite membranes were capable of excluding over 90% polyethylene glycol 400′corresponding to a Stokes radius of 0.518 nm. The performances of some similar state-of-the-art membranes based on PIP are shown in Table 2 for comparison. Obviously, the composite membrane in this study showed an excellent property.

### 3.3. Stability and anti-fouling performance of membranes

To evaluate the stability and antifouling performance, membranes were subjected to a pure water permeation test

Table 2
Performance of the PIP/TMC-based MMMs for nanofiltration in recent researches

| Filler | Performance | | | | | Test condition | Ref. |
|---|---|---|---|---|---|---|---|
| | Permeability ($L\ h^{-1}\ m^{-2}\ bar^{-1}$) | Rejection (%) | | | | | |
| | | $Na_2SO_4$ | $MgSO_4$ | NaCl | $MgCl_2$ | | |
| Hollow PPy nanoparticle | 18.2[a] | 98.4 | 99.3 | 49.0 | 67.5 | Room temperature, 0.5 MPa, 1 g $L^{-1}$ | This study |
| GO | 14.6[a] | 98.2 | 96.5 | 56.8 | 50.5 | 25°C, 2,000 ppm, and 0.6 MPa | [38] |
| GO | 6.9[a] | 96.8 | 85.4 | 32.1 | 76.8 | 25°C, 0.6 MPa, and 2,000 ppm | [39] |
| Maleic anhydride modified GO | 8.2[a] | 98.0 | 89.0 | 32.3 | 76.8 | | |
| GO | 5.5[a] | 89.9 | | 33.0 | | 25°C, 1.0 MPa, and 2,000 ppm | [40] |
| Reduced GO-$TiO_2$ | 6.1[a] | 93.6 | | 36.6 | | | |
| Maleic anhydride modified GO | 14.3[b] | 98.0 | | | | 25°C ± 1°C, 0.6 MPa | [41] |
| Perbranched polymer functionalized GO | 8.0[a] | 99.0 | 96.3 | 66.8 | 84.7 | 25°C ± 1°C, 0.6 MPa | [42] |
| Zwitterions functionalized MWCNT | 12.3[a] | 97.6 | 94.1 | 18.2 | 60.4 | 25°C, 0.6 MPa | [43] |
| Oxidized multi-walled carbon nanotubes (MWCNT) | 7.6[b] | 97.9 | | | | 25°C, 1.0 MPa, and 2,000 ppm | [25] |
| Poly(methyl methacrylate) functionalized MWCNT | 7.0[a] | 99.0 | | 44.1 | | 20°C, 1.0 MPa, and 2,000 ppm | [44] |
| MWCNT-COOH | 6.2[a] | 96.6 | 93.7 | 34 | | 20°C ± 0.5°C, 0.6 MPa, and 2,000 ppm | [45] |
| MWCNT-OH | 6.9[a] | 97.6 | 97.1 | 35.3 | | | |
| MWCNT-$NH_2$ | 5.3[a] | 96.8 | 95 | 35.5 | | | |
| Sulfonated MWCNT | 13.2[a], 11.5–10.4[b] | 96.8 | 91.1 | 45.5 | 62.4 | Room temperature, 0.6 MPa, 1 g $L^{-1}$ | [46] |
| Carboxylated MWCNT | 8.8–10.0[b] | | 98.5 | 18.5 | | 25°C, 0.7 MPa, 2 g $L^{-1}$ $MgSO_4$, or 1 g $L^{-1}$ NaCl | [47] |
| ZnO nanospheres | 4.3–6.7[b] | | 92.2 | 22.8 | | 25°C, 0.7 MP, and 1,000 ppm | [48] |
| Polydopamine nanoparticle | 9.9[a] | 98.1 | 97.9 | 43.1 | 44.1 | Room temperature, 0.6 MPa, 1,000 ppm | [5] |
| Sulfonated carbon quantum dots | 7.0[a] | 93.6 | 85.4 | 7.3 | 31.7 | 0.35 MPa, 5 mmol $L^{-1}$ | [10] |
| $Al(OH)_3$ nanosphere | 4.6–5.2[b] | | 94.9 | 27.6 | | 25°C, 0.7 MPa, and 1 g $L^{-1}$ | [49] |
| $SiO_2$ nanosphere | 4.5[b] | | 94.8 | | | 25°C, 0.5 MPa, and 2,000 ppm | [50] |
| $SiO_2$ nanoparticle | 9.5[b] | 97.3 | 91.1 | 25.6 | 50.7 | 25°C ± 0.5°C, 0.6 MPa, and 2,000 ppm | [51] |
| $TiO_2$ nanosphere | 5.1[a] | 89.1 | | 35.6 | | 25°C, 1.0 MPa, and 2,000 ppm | [40] |
| $TiO_2$ nanosphere | 2.6[b] | | 96.9 | | | 25°C, 0.5 MPa, and 2,000 ppm | [52] |
| $Fe_2O_3/SiO_2$ nanoparticles | 3.2[a] | 85.0 | | 30.1 | | Room temperature, 0.6 MPa, 1,000 mg $L^{-1}$ | [53] |
| MIL-53 | 6.9[b] | | | 40.4 | | 20°C ± 1°C, 1.0 MPa, and 10 mmol $L^{-1}$ | [24] |
| $NH_2$-UiO-66 | 7.2[b] | | | 42.2 | | | |
| ZIF-8 | 7.1[b] | | | 35.4 | | | |
| Mesoporous $SiO_2$ (SBA-15) | 4.6[b] | | 85.2 | | | 20°C, 1.0 MPa, and 2,000 ppm | [54] |

[a]Pure water permeability.
[b]Salt solution permeability.

and a HA solution permeation test, respectively. The absolute and normalized fluxes of the composite membranes were exhibited in Fig. 11. During the running time of 840 min, the pure water flux of the unmodified composite membrane always remained above 96% of initial flux, while that of the membranes modified with 0.01% HPNs was down to 89%, indicating the limitation of the physical blending of the fillers (the instability). In HA solution, the flux of unmodified membranes decreased to 82% and that of modified membranes decreased to 86%. By comparing the decrease in pure water flux and in HA solution flux, we could conclude that the incorporation of the HPNs was beneficial to the improvement of membrane antifouling performance. Although the decrease in electronegativity of the membrane surface was unfavorable to the improvement of antifouling performance, because of the increased affinity between the HA and the membrane surface since HA was electronegative in the water. Thus, the flux of the modified membranes decreased sharply in the initial stage due to the adsorption of HA in the surface with lower electronegativity. In the next stage, the improved hydrophilicity of membrane surface, which was unfavorable to deposition, led to the improved antifouling performance. Thus, the flux of modified membrane tended to an equilibrium state rapidly, while that of unmodified membranes decreased gradually. Even at the end of the fouling experiment, the flux of the modified membranes did not reach the equilibrium. Regardless, even we found the instability induced by the physical combination between the fillers and the matrix, the fluxes of the membranes modified with HPNs were significantly higher than those of unmodified membranes as shown in Fig. 11a. After the 840 min pollution test, the cleaning process was conducted, the result showed no significant water flux recovery when washed with deionized water and citric acid solution as shown in Fig. 12. The water flux increased slightly compared with that before cleaning process. The flux recovery increased after washed with NaOH solution. And the flux recovery ratio for modified membranes was 91%, up slightly from 86% for unmodified membranes. The cleaning process for both membranes did not achieve the ideal effect, indicating the formation of the compact gel layer.

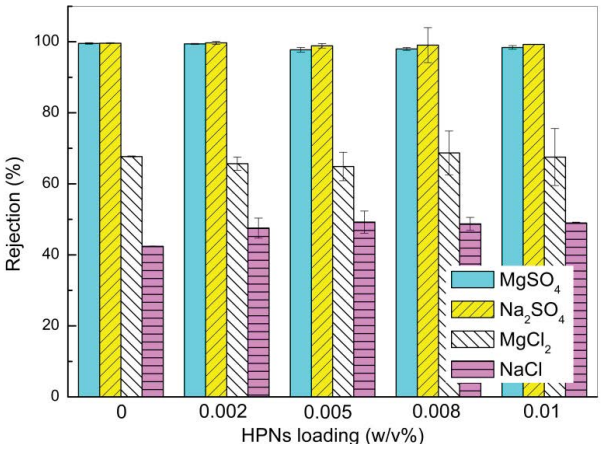


Fig. 10. Effect of the HPNs on the rejections of the composite membranes

## 4. Conclusion

PIP based composite membranes were modified by mixing the hollow polypyrrole nanoparticles into the selective layer. The incorporation of the hollow nanospheres led to the decreased degree of cross-linking and zeta potential with the increased surface roughness and hydrophilicity. The permeability significantly increased, the pure water flux more than doubled. The rejections of the inorganic salts showed a small fluctuation, except NaCl with a 12% rise. In addition, the antifouling performance against HA was improved. However, the instability of the performance with an 11% decrement in pure water flux during 840 min induced by physical blending modification also appeared in this study. Consequently, we will introduce the hollow polypyrrole nanospheres into membranes by chemical modification to improve the stability in the near future.

## Acknowledgments

This work was supported by the National Natural Science Foundation of China (Grant No. 21776217 and 21978214), National Key Research and Development Plan

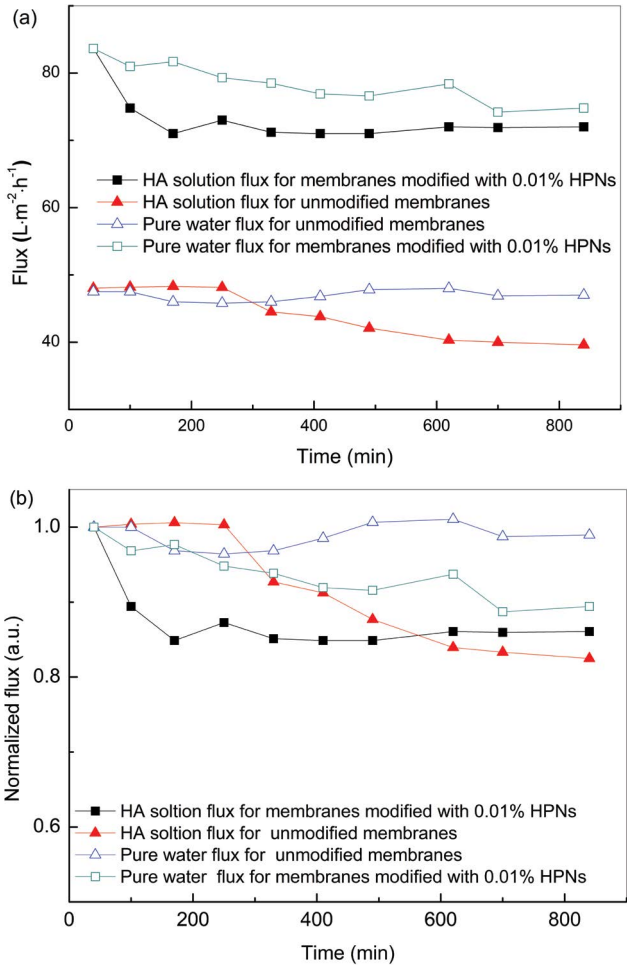


Fig. 11. Time dependence of the pure water flux and the HA solution flux for the composite membranes. (a) Flux and (b) Normalized flux.

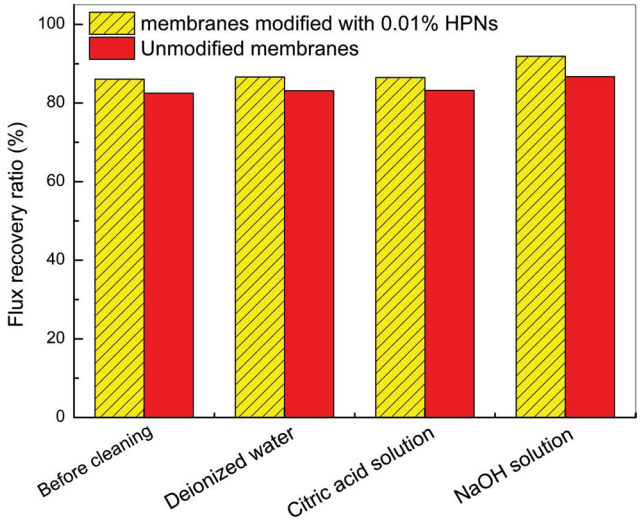


Fig. 12. Cleaning effects of different cleaning agents.

(2017YFC0404001), Tianjin Natural Science Foundation (No. 18JCYBJC89400), and Technology Plans of Tianjin (No. 17PTSYJC00050 and 18PTSYJC 00190).

## References

[1] H.B. Park, J. Kamcev, L.M. Robeson, M. Elimelech, B.D. Freeman, Maximizing the right stuff: the trade-off between membrane permeability and selectivity, Science, 356 (2017) 1138–1148.
[2] Z. Zhang, G.D. Kang, H.J. Yu, Y. Jin, Y.M. Cao, Fabrication of a highly permeable composite nanofiltration membrane via interfacial polymerization by adding a novel acyl chloride monomer with an anhydride group, J. Membr. Sci., 570–571 (2019) 403–409.
[3] Y.L. Ji, W.J. Qian, Y.W. Yu, Q.F. An, L.F. Liu, Y. Zhou, C.J. Gao, Recent developments in nanofiltration membranes based on nanomaterials, Chin. J. Chem. Eng., 25 (2017) 1639–1652.
[4] K. Sunil, G. Karunakaran, S. Yadav, M. Padaki, V. Zadorozhnyy, R.K. Pai, Al-$Ti_2O_6$ a mixed metal oxide based composite membrane: a unique membrane for removal of heavy metals, Chem. Eng. J., 348 (2018) 678–684.
[5] M.B.M.Y. Ang, Y.-L. Ji, S.-H. Huang, K.-R. Lee, J.-Y. Lai, A facile and versatile strategy for fabricating thin-film nanocomposite membranes with polydopamine-piperazine nanoparticles generated *in situ*, J. Membr. Sci., 579 (2019) 79–89.
[6] J.D. Liu, W.R. Mu, J.T. Wang, H. Liu, Y.T. Qin, J. He, F. Guo, Y. Li, Y.F. Li, X.Z. Cao, P. Zhang, E. Lu, Polydopamine-enabled distribution of polysiloxane domains in polyamide thin-film nanocomposite membranes for organic solvent nanofiltration, Sep. Purif. Technol., 205 (2018) 140–150.
[7] Y.Y. Li, C. Li, S.X. Li, B.W. Su, L.H. Han, B. Mandal, Graphene oxide (GO)-interlayered thin-film nanocomposite (TFN) membranes with high solvent resistance for organic solvent nanofiltration (OSN), J. Mater. Chem. A, 7 (2019) 13315–13330.
[8] N. Gholami, H. Mahdavi, Nanofiltration composite membranes of polyethersulfone and graphene oxide and sulfonated graphene oxide, Adv. Polym. Technol., 37 (2018) 3529–3541.
[9] Z.-X. Low, J. Ji, D. Blumenstock, Y.-M. Chew, D. Wolverson, D. Mattia, Fouling resistant 2D boron nitride nanosheet-PES nanofiltration membranes, J. Membr. Sci., 563 (2018) 949–956.
[10] H.Z. Sun, P.Y. Wu, Tuning the functional groups of carbon quantum dots in thin film nanocomposite membranes for nanofiltration, J. Membr. Sci., 564 (2018) 394–403.
[11] R. Abedini, Enhanced antifouling properties of poly (ethersulfone) nano-composite membrane filled with nano-clay particles, Polym. Bull., 76 (2019) 1737–1753.
[12] M.L. Lind, A.K. Ghosh, A. Jawor, X.F. Huang, W. Hou, Y. Yang, E.M.V. Hoek, Influence of zeolite crystal size on zeolite-polyamide thin film nanocomposite membranes, Langmuir, 25 (2009) 10139–10145.
[13] F. Xiao, B. Wang, X.Y. Hu, S. Nair, Y.B. Chen, Thin film nanocomposite membrane containing zeolitic imidazolate framework-8 via interfacial polymerization for highly permeable nanofiltration, J. Taiwan Inst. Chem. Eng., 83 (2018) 159–167.
[14] C. Echaide-Gorriz, M. Navarro, C. Tellez, J. Coronas, Simultaneous use of MOFs MIL-101(Cr) and ZIF-11 in thin film nanocomposite membranes for organic solvent nanofiltration, Dalton Trans., 46 (2017) 6244–6252.
[15] G.H. Zhu, F.Y. Zhang, M.P. Rivera, X.X. Hu, G.Y. Zhang, C.W. Jones, R.P. Lively, Molecularly mixed composite membranes for advanced separation processes, Angew. Chem. Int. Ed., 58 (2019) 2638–2643.
[16] S.K. Das, P. Manchanda, K.-V. Peinemann, Solvent-resistant triazine-piperazine linked porous covalent organic polymer thin-film nanofiltration membrane, Sep. Purif. Technol., 213 (2019) 348–358.
[17] Ihsanullah, Carbon nanotube membranes for water purification: developments, challenges, and prospects for the future, Sep. Purif. Technol., 209 (2019) 307–337.
[18] M.H.D.A. Farahani, D. Hua, T.-S. Chung, Cross-linked mixed matrix membranes (MMMs) consisting of amine-functionalized multi-walled carbon nanotubes and P84 polyimide for organic solvent nanofiltration (OSN) with enhanced flux, J. Membr. Sci., 548 (2018) 319–331.
[19] Z.F. Gao, Y.N. Feng, D.C. Ma, T.-S. Chung, Vapor-phase crosslinked mixed matrix membranes with UiO-66-$NH_2$ for organic solvent nanofiltration, J. Membr. Sci., 574 (2019) 124–135.
[20] G.P.S. Ibrahim, A.M. Isloor, A. Moslehyani, A.F. Ismail, Bio-inspired, fouling resistant, tannic acid functionalized halloysite nanotube reinforced polysulfone loose nanofiltration hollow fiber membranes for efficient dye and salt separation, J. Water Process. Eng., 20 (2017) 138–148.
[21] M. Salimi, V. Pirouzfar, Preparation and characterization of a novel MMMs by comprising of PSF-HNT/$TiO_2$ nanotubes to reduce organic sediments, Polym. Bull., 75 (2018) 2285–2299.
[22] J.Y. Zhu, N.N. Guo, Y.T. Zhang, L. Yu, J.D. Liu, Preparation and characterization of negatively charged PES nanofiltration membrane by blending with halloysite nanotubes grated with poly (sodium 4-styrenesulfonate) via surface-initiated ATRP, J. Membr. Sci., 465 (2014) 91–99.
[23] A. Sumisha, G. Arthanareeswaran, A.F. Ismail, D.P. Kumar, M.V. Shankar, Functionalized titanate nanotube-poly-etherimide nanocomposite membrane for improved salt rejection under low pressure nanofiltration, RSC Adv., 5 (2015) 39464–39473.
[24] Y.-Y. Zhao, Y.-L. Liu, X.-M. Wang, X. Huang, Y.F. Xie, Impacts of metal-organic frameworks on structure and performance of polyamide thin-film nanocomposite membranes, ACS Appl. Mater. Interface, 11 (2019) 13724–13734.
[25] M.R. Mahdavi, M. Delnavaz, V. Vatanpour, Fabrication and water desalination performance of piperazine-polyamide nanocomposite nanofiltration membranes embedded with raw and oxidized MWCNTs, J. Taiwan Inst. Chem. Eng., 75 (2017) 189–198.
[26] C.W. Zhao, B. Yang, J.L. Han, Y.Y. Meng, L. Yu, D.Y. Hou, J. Wang, Y. Zhao, Y.H. Zhai, S.G. Wang, X.F. Sun, Preparation of carboxylic multiwalled-carbon-nanotube-modified poly (m-phenylene isophthalamide) hollow fiber nanofiltration membranes with improved performance and application for dye removal, Appl. Surf. Sci., 453 (2018) 502–512.
[27] K. Sears, L. Dumée, J. Schütz, M. She, C. Huynh, S. Hawkins, M. Duke, S. Gray, Recent developments in carbon nanotube membranes for water purification and gas separation, Materials, 3 (2010) 127–149.
[28] X.L. Wang, X.L. Ding, H.Y. Zhao, J.X. Fu, Q.P. Xin. Y.Z. Zhang, Pebax-based mixed matrix membranes containing hollow polypyrrole nanospheres for enhanced gas permeation

performance, J. Membr. Sci., 602 (2020), doi: 10.1016/j.memsci.2020.117968.
[29] K.Y. Wang, T.-S. Chung, The characterization of flat composite nanofiltration membranes and their applications in the separation of Cephalexin, J. Membr. Sci., 247 (2005) 37–50
[30] H.F. Tan, J.J. Li, X.Y. Yue, M. Wang, Q.M. Pan, ATR-FTIR and XPS surface analysis techniques for commercial polyamide membranes, Membr. Sci. Technol., 35 (2015) 22–27.
[31] M. Omastová, M. Trchová, J. Kovářová, J. Stejskal, Synthesis and structural study of polypyrroles prepared in the presence of surfactants, Synth. Met., 138 (2003) 447–455.
[32] Y.F. Li, Y.L. Su, Y.N. Dong, X.T. Zhao, Z.Y. Jiang, R.N. Zhang, J.J. Zhao, Separation performance of thin-film composite nanofiltration membrane through interfacial polymerization using different amine monomers, Desalination, 333 (2014) 59–65.
[33] F. Yuan, Formation Visualization of Interfacially Polymerized Film and Preparation of Composite Membrane for $CO_2$ Separation, Tianjin University, Tianjin, 2012.
[34] B. Majhy, R. Iqbal, A.K. Sen, Facile fabrication and mechanistic understanding of a transparent reversible superhydrophobic-superhydrophilic surface, Sci. Rep., 8 (2018), doi: 10.1038/s41598-018-37016-5.
[35] J.L. Yong, F. Chen, Q. Yang, J.L. Huo, X. Hou, Superoleophobic surfaces, Chem. Soc. Rev., 46 (2017) 4168–4217.
[36] M. Nie, F. Huang, Z.G. Wang, C.Y. Ning, Construction and anti-bacteria adhesion properties of polypyrrole nanostructures on 304 stainless steel surface, Surf. Technol., 48 (2019) 210–216.
[37] Y.J. Zeng, L.H. Wang, L. Zhang, J.Q. Yu, An acid resistant nanofiltration membrane prepared from a precursor of poly(s-triazine-amine) by interfacial polymerization, J. Membr. Sci., 546 (2018) 225–233.
[38] J. Wang, C.W. Zhao, T. Wang, Z. Wu, X. Li, J.D. Li, Graphene oxide polypiperazine-amide nanofiltration membrane for improving flux and anti-fouling in water purification, RSC Adv., 6 (2016) 82174–82185.
[39] Q.L. Xie, S.S. Zhang, Z. Hong, H.J. Ma, B.R. Zeng, X. Gong, W.Y. Shao, Q.Q. Wang, A novel double-modified strategy to enhance the performance of thin-film nanocomposite nanofiltration membranes: incorporating functionalized graphenes into supporting and selective layers, Chem. Eng. J., 368 (2019) 186–201.
[40] M. Safarpour, V. Vatanpour, A. Khataee, M. Esmaeili, Development of a novel high flux and fouling-resistant thin film composite nanofiltration membrane by embedding reduced graphene oxide/$TiO_2$, Sep. Purif. Technol., 154 (2015) 96–107.
[41] Q.L. Xie, W.Y. Shao, S.S. Zhang, Z. Hong, Q.Q. Wang, B.R. Zeng, Enhancing the performance of thin-film nanocomposite nanofiltration membranes using MAH-modified GO nanosheets, RSC Adv., 7 (2017) 54898–54910.
[42] Q.L. Xie, S.S. Zhang, H.J. Ma, W.Y. Shao, X. Gong, Z. Hong, A novel thin-film nanocomposite nanofiltration membrane by incorporating 3D hyperbranched polymer functionalized 2D graphene oxide, Polymers, 10 (2018), doi: 10.3390/polym10111253.
[43] Y.-S. Guo, Y.-F. Mi, F.-Y. Zhao, Y.-L. Ji, Q.-F. An, C.-J. Gao, Zwitterions functionalized multi-walled carbon nanotubes/polyamide hybrid nanofiltration membranes for monovalent/divalent salts separation, Sep. Purif. Technol., 206 (2018) 59–68.
[44] J.N. Shen, C.C. Yu, H.M. Ruan, C.J. Gao, B. Van der Bruggen, Preparation and characterization of thin-film nanocomposite membranes embedded with poly(methyl methacrylate) hydrophobic modified multiwalled carbon nanotubes by interfacial polymerization, J. Membr. Sci., 442 (2013) 18–26.
[45] S.M. Xue, Z.L. Xu, Y.J. Tang, C.H. Ji, Polypiperazine-amide nanofiltration membrane modified by different functionalized multiwalled carbon nanotubes (MWCNTs), ACS Appl. Mater. Interface, 8 (2016) 19135–19144.
[46] J.F. Zheng, M. Li, K. Yu, J.H. Hu, X. Zhang, L.J. Wang, Sulfonated multiwall carbon nanotubes assisted thin-film nanocomposite membrane with enhanced water flux and anti-fouling property, J. Membr. Sci., 524 (2017) 344–353.
[47] H.B. Li, W.Y. Shi, Y.H. Su, H.X. Zhang, X.H. Qin, Preparation and characterization of carboxylated multiwalled carbon nanotube/polyamide composite nanofiltration membranes with improved performance, J. Appl. Polym. Sci., 134 (2017), doi: /10.1002/app.45268.
[48] H.B. Li, W.Y. Shi, H.Y. Zhu, Y.F. Zhang, Q.Y. Du, X.H. Qin, Effects of zinc oxide nanospheres on the separation performance of hollow fiber poly(piperazine-amide) composite nanofiltration membranes, Fibers Polym., 17 (2016) 836–846.
[49] H.B. Li, W.Y. Shi, Y.F. Zhang, Q.Y. Du, X.H. Qin, Y.H. Su, Improved performance of poly(piperazine amide) composite nanofiltration membranes by adding aluminum hydroxide nanospheres, Sep. Purif. Technol., 166 (2016) 240–251.
[50] Q. Li, Y.H. Wang, J. Song, Y.P. Guan, H. Yu, X.H. Pan, F.Y. Wu, M. Zhang, Influence of silica nanospheres on the separation performance of thin film composite poly(piperazine-amide) nanofiltration membranes, Appl. Surf. Sci., 324 (2015) 757–764.
[51] D. Hu, Z.L. Xu, C. Chen, Polypiperazine-amide nanofiltration membrane containing silica nanoparticles prepared by interfacial polymerization, Desalination, 301 (2012) 75–81.
[52] Q. Wang, G.S. Zhang, Z.-S. Li, S. Deng, H. Chen, P. Wang, Preparation and properties of polyamide/titania composite nanofiltration membrane by interfacial polymerization, Desalination, 352 (2014) 38–44.
[53] Y. Mansourpanah, A. Rahimpour, M. Tabatabaei, L. Bennett, Self-antifouling properties of magnetic $Fe_2O_3/SiO_2$-modified poly (piperazine amide) active layer for desalting of water: characterization and performance, Desalination, 419 (2017) 79–87.
[54] Q. Li, Z.K. Li, H. Yu, X.H. Pan, X.L. Wang, Y.H. Wang, J. Song, Effects of ordered mesoporous silica on the performances of composite nanofiltration membrane, Desalination, 327 (2013) 24–31.